Hindawi
Journal of Robotics
Volume 2020, Article ID 8860550, 13 pages
https://doi.org/10.1155/2020/8860550

Research Article

Development and Performance Analysis of Pneumatic Soft-Bodied Bionic Basic Execution Unit

Yu Zhang, Wenchuan Zhao, Ning Wang, and Dengyu Lu

School of Mechanical Engineering, Shenyang University of Technology, Shenyang 110870, China

Correspondence should be addressed to Wenchuan Zhao; zhangyu@sut.edu.cn

Received 12 July 2020; Revised 1 October 2020; Accepted 20 October 2020; Published 3 November 2020

Academic Editor: Ramadoni Syahputra

This paper studies the design of pneumatic soft-bodied bionic basic execution unit with soft-rigid combination, which can be used as an actuator for pneumatic soft-bodied robots and soft-bodied manipulators. This study is inspired by structural characteristics and motion mechanism of biological muscles, combined with the nonlinear hyperelasticity of silica gel and the insertion of thin leaf spring structure in the nonretractable layer. Response surface analysis and numerical simulation algorithm are used to determine the optimal combination of structural dimension parameters by taking the maximum output bending angle of the basic executing unit as the optimization objective. Based on Odgen's third-order constitutive model, the deformation analysis model of the basic execution unit is established. The physical model of pneumatic soft-bodied bionic basic execution unit is prepared through 3D printing, shape deposition, soft lithography, and other processing methods. Finally, the motion and dynamic characteristics of the physical model are tested through experiments and result analysis, thus obtaining curves and empirical formulas describing the motion and dynamic characteristics of the basic execution unit. The relevant errors are compared with the deformation analysis model of the execution unit to verify the feasibility and effectiveness of the design of the pneumatic soft-bodied bionic basic execution unit. The above research methods, research process, and results can provide a reference for the research and implementation of pneumatic and hydraulic driven soft-bodied robots and grasping actuators of soft-bodied manipulators.

1. Introduction

With the increasing requirements for robotic flexibility, the disadvantages of traditional rigid robots are gradually highlighted, such as their heavy structure, low safety factors, poor environmental adaptability, loud noise, and their limited ability to interact with natural environment or human beings. While traditional rigid robots can no longer fully meet the development needs in various fields, natural organisms provide new ideas for the development of robots with their soft body, excellent flexibility, and strong environmental adaptability [1–5]. Therefore, to further expand the functions and applications of robots, soft-bodied bionic robots have become a new direction in the field of robotics. This kind of robot is mainly made of soft or malleable materials; it can continuously deform in a limited space by simulating the muscle motion of the natural organisms. Compared with traditional rigid robots, it has infinite degrees of freedom and can show unprecedented flexibility, safety, and agility [6, 7].

At present, the most widely used soft-bodied robots are pneumatic and hydraulic driven soft bionic robots, which are diverse in types and structural forms, with the characteristics of fast response, high driving force, high power density, and so on. Suzumori et al. [8] from Okayama University have developed a soft manta ray robot. The body material of the robot is silicone rubber, with a body length of 150 mm, a body width of 170 mm, and the maximum swimming speed of 100 mm/s. Marchese et al. [9] from Massachusetts Institute of Technology have developed a new kind of pneumatic soft-bodied bionic robotic fish. The actuator is made from silicone rubber material, which can achieve swift maneuvers in the underwater environment and track the target object. Tolley et al. [10] from Harvard University have designed the world's first pneumatic soft-bodied crawling robot with limbs and trunks composed of all

soft elastic materials. It can achieve two kinds of gait: undulating wave and crawling. Marchese et al. [11] from Massachusetts Institute of Technology have designed a multi-degree-of-freedom pneumatic soft-bodied manipulator with good compliance performance. In narrow spaces, it can achieve flexible operation by adjusting the body posture and can avoid damage to the surrounding environment. Hao et al. [4] from Beihang University have designed a pneumatic four-fingered soft-bodied manipulator. By inflating and deflating, the target object can be grasped and released, and the length of the body structure can be adjusted to achieve multiobject grasping. Li et al. [12] from Harvard University have developed a soft-bodied bionic manipulator based on the contraction and relaxation principle of human muscles, which can grasp objects weighing less than 3 kg. Liming et al. [13] from Harbin Engineering University have designed a soft-bodied crawling robot based on the mechanical properties of soft materials and the relation between friction and driving force, and it can be used to maneuver specifically in planes and pipelines. Phillips et al. [14] from NSF Biological Development Agency have designed a soft manipulator. The pressure of the soft cavity structure can be controlled by the pressure proportional valve, so that it can achieve flexible operation in deep-sea. Frame et al. [15] from Atlantic University of Florida have developed a water-injection driven artificial jellyfish based on soft materials. By injecting certain pressure into the inner part of the soft-propulsive tentacle, the tentacle can imitates the swimming posture of jellyfish through bending deformation and can swim in narrow spaces. Jiantao et al. [16] from Yanshan University have designed a wheeled-foot peristaltic soft-bodied bionic robot with a double-cavity structure. It inflates and deflates periodically through the airbag structure, bends the body structure, and achieves the rapid motion of the robot by introducing a wheel-foot design.

All the above-mentioned soft-bodied robots are designed to imitate biological characteristics and make full use of the advantages of soft materials, which simplifies the structure of the robot body, while greatly improving their environment the adaptability. These researches have broadened the application field of soft-bodied bionic robots, but they still inevitably rely on the character analysis of soft-bodied bionic basic execution unit.

Bishop-Moser et al. [17, 18] from Villamora in Portugal have established a theoretical model of the interaction between incompressible liquids, nonstretchable filament, and the body of hydraulic driven soft-bodied basic execution unit, which can accurately predict the deformation direction of soft-bodied basic execution unit. According to their numerical simulation and experimental research, Mosadegh et al. [19] from Harvard University have determined the relationship between the inflation pressure and the motion characteristics of the pneumatic soft-bodied basic execution unit and proved that the bending amplitude depends on the bending path. Luo et al. [20] from Worcester Institute of Technology have studied the dynamic response of hydraulic driven soft-bodied execution unit through visual tracking system and proved that quick response and good robustness are achieved under higher pressure. Peele et al. [21] from Cornell University have determined the material properties of pneumatic soft-bodied bionic actuator through rheological principle and tensile test, followed by numerical simulations aiming to reduce the stress concentration of the actuator and increase the motion amplitude. Connolly et al. [22] from Harvard University have determined the relationship between the filament winding angle and the deformation of the pneumatic soft-bodied actuator through numerical simulation technology, so that the actuator can achieve different motion forms. Finally, multiple actuators were connected in series to develop a worm-like soft-bodied robot. Pengzhan et al. [23] from East China Jiaotong University controlled the pressure values of the chamber by collecting and processing the internal pressure and bending angle signals of the pneumatic soft-bodied execution unit and changed the bending angle of the execution unit, thus evaluating its performance in different motion states, and ensured its good flexibility and environmental adaptability. Based on the motion mechanism of fish muscle, Jusufi et al. [24] from the University of Technology Sydney have established a passive flexible mechanical model of the pneumatic soft-bodied underwater execution unit. Then, by controlling the flexible foil embedded in the body, the motion mechanism and stiffness change of the execution unit were studied. Finally, according to the movement phase and frequency of the execution unit, the changing rule of the thrust generated by the execution unit was determined, which provides a reference for the application of underwater carrier. Liming et al. [25] from Harbin Engineering University have analyzed the static characteristics of multi cavity type pneumatic soft-bodied bionic actuator and verified the feasibility of the actuator design principle. Based on the rowing propulsion of frog swimming, Jizhuang et al. [26] from Harbin Institute of Technology put forward a kind of joint type pneumatic soft-bodied actuator unit. Firstly, according to the Yeoh constitutive model and virtual work principle, combined with the geometric parameters of the actuator unit, the deformation analysis model is established. Then, the bending angle and load torque of the actuator unit were studied through different winding forms of the filament, which provides a feasible reference for the development of the frog-like swimming robot. Chen et al. [27] from Tianjin University have analyzed the static characteristics of the pneumatic soft-bodied actuator by using the virtual work principle and then deducted and solved the deflection function of the actuator surface by Rayleigh Ritz method. Finally, the deformation error of the actuator was determined to be low by connecting the deformation of the actuator with the surface deformation of the soft robot. It can be proved that it is feasible to study the deformation of the soft actuator based on the principle of virtual work and the principle of minimum potential energy and that this approach can simplify the mathematical model of the soft-bodied actuator. Azami et al. [28] from Tokyo Medical University have designed a pneumatic soft-bodied actuator composed of silica gel and metal spring. The oscillation circuit was connected to the spring inside the actuator. According to the change of spring length, the corresponding

spring oscillation frequency was measured. Through the oscillation frequency, the displacement output of the actuator could be determined, so as to realize the motion control of the soft-bodied actuator. Saleh et al. [29] from Nile University have studied the slope angle of the expansion wall of the pneumatic soft-bodied actuator and determined the relationship among inflation pressure, motion range, and reaction force of the soft-bodied actuator through nonlinear static finite element analysis. The feasibility of the design of the soft-bodied actuator is verified by using the load scale in the experiment, proving that the design can meet the grasping requirements of the soft-bodied manipulator.

Although the above-mentioned scholars in related fields have done numerous works on the pneumatic soft-bodied bionic basic execution unit, the theoretical model of the pneumatic soft-bodied bionic basic execution unit needs further exploration, and the research on the motion and dynamic characteristics still need further systematization and perfection. Besides, most of the researches are limited to the type of entirely soft-bodied or filament + soft-bodied, which calls for the improvement of structure strength, execution strength, and resilience of the pneumatic soft-bodied bionic basic execution unit, making it difficult to lay a good foundation for further application. Therefore, this paper has achieved a certain extent of innovation in the structure design, optimal combination of structure parameters, establishment of mechanical model, physical model preparation, analysis of motion characteristics, and analysis of dynamic characteristics of the pneumatic soft-bodied bionic basic execution unit with soft-rigid combination. The research process is innovative, systematic, and universally applicable.

2. Structure Design and Motion Mechanism Analysis

2.1. Design Basis. Based on the hyperelastic characteristics of the silica gel material and muscle motion mechanism, referring to the crawling form of inchworm in nature, the swimming form of fishtail with swinging trunk, and the grasping form of arm and elephant trunk, a pneumatic soft-bodied bionic basic execution unit of the soft-rigid combination is designed. By inflating the interior of the basic execution unit cavity structure, each cavity can be inflated and extruded. Combined with different inflations pressure values, the execution unit can realize periodic bending movement and power output. In this process, to enhance the structural strength, execution force, and motion recovery force of the soft-bodied basic execution unit, a thin leaf spring structure is embedded in the nonretractable layer, which can not only avoid the axial extension of the nonretractable layer with the cavity expansion but also improve the structure strength, execution strength and resilience of the basic execution unit and therefore further improve the overall performance and broaden the application fields of the pneumatic soft-bodied bionic basic execution unit.

2.2. Structure Design. At present, the cavity structure shape types of the pneumatic soft-bodied bionic basic execution unit generally include rectangle, semiellipse, bow, fan, and triangle. The application scenarios of different shapes are different, and only the cavity structures of different shapes need to be designed according to specific situations. It should be noted that when the cavity structure of the basic executing unit expands, its structure shape has little influence on its motion frequency, bending angle, and driving load, but the parameters combination of its specific structure size plays a key role. Therefore, in this paper, the soft-bodied bionic basic execution unit of the rectangular cavity structure, which is the most widely used and universal representative, is taken as an example to study its motion and dynamic characteristics.

The structure design of the pneumatic soft-bodied bionic basic execution unit is shown in Figure 1. Its structure is mainly composed of soft-bodied cavity, nonretractable layer, and thin leaf spring.

The structure dimensions of the basic execution unit are shown in Table 1. It should be noted that to ensure the effectiveness of the expansion wall of the basic execution unit, the remaining wall of the cavity structure should be thicker than the expansion wall.

3. Optimal Combination of Structural Parameters

The combination of structural dimension parameters plays a key role in the motion and dynamic characteristics of the pneumatic soft-bodied bionic basic execution unit. To shorten the experimental research period and reduce experimental cost, the optimal combination of structural parameters is studied based on the response surface analysis method [30–34] and numerical simulation algorithm [35–38]. According to the design principle of the Box-Behnken central composite experiment, the maximum bending angle Φ is used for determining the optimum extraction process. Among them, the maximum bending angle Φ is determined using numerical simulation algorithm, as shown in Figure 2.

In this paper, the response surface analysis experiments of 8 factors and 3 levels are designed based on the specific structure size of the basic execution unit, as shown in Table 2.

120 groups of experiments can be obtained from 8 factors and 3 levels of response surface analysis tests in Table 2. According to the experimental parameters of each group, the corresponding numerical analysis model is constructed by the numerical simulation algorithm, and the maximum bending angles Φ corresponding to the experimental parameters of each group are obtained, respectively. Then, regression analysis was carried out from the data obtained, and the quadratic polynomial regression equation of bending angle Φ was fitted as in the following:

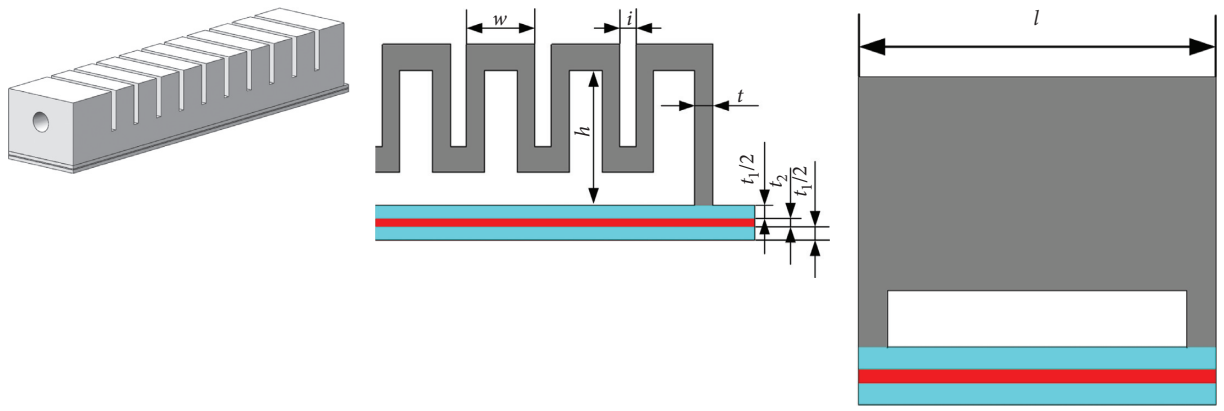

Figure 1: Structure design of pneumatic soft-bodied bionic basic execution unit. (a) 3D digital model. (b) Longitudinal local cross section. (c) Transverse local cross section.

Table 1: Dimensions of pneumatic soft-bodied bionic basic execution unit.

No.	Size
1	Single cavity length l
2	Single cavity width w
3	Single cavity height h
4	Thickness of expansion wall of single cavity t
5	Nonretractable layer thickness t_1
6	Thickness of thin leaf spring t_2
7	Cavity spacing i
8	Total number of cavity N

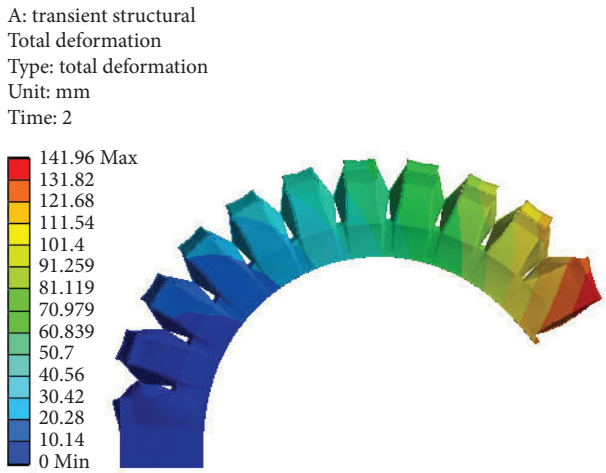

Figure 2: Numerical simulation calculation results of pneumatic soft-bodied bionic basic execution unit. The inflation pressure is constant at 180 kpa.

Table 2: Level and coding of test factors in response surface.

Coding	l	w	h	t	t_1	t_2	i	N
−1	22	7	14	0.8	1.8	0.3	1.2	9
0	26	9	16	1.0	2.1	0.4	1.3	11
1	30	11	18	1.2	2.4	0.5	1.4	13

$$\begin{aligned} R = {} & 2.11 + 4.161E - 0.03A + 0.055B - 0.045C - 0.17D \\ & - 0.16F + 0.37G + 0.19H + 0.026AB - 0.090AC \\ & - 0.085AD + 0.14AE - 0.18AF - 0.017AG \\ & - 0.081AH - 0.073BC + 0.050BD + 0.10BE \\ & - 0.23BF + 0.080BG - 0.017BH + 0.12CD + 0.11CE \\ & - 0.023CF - 0.013CG + 0.090CH + 0.18DE \\ & - 0.060DF - 0.076DG + 0.050DH - 0.031EF \\ & + 0.059EG - 0.037EH - 0.068FG - 0.14FH \\ & + 0.053GH - 0.27A2 - 0.37B2 - 0.19C2 - 0.21D2 \\ & - 0.11E2 - 0.18F2 - 0.29G2 - 0.051H2, \end{aligned} \tag{1}$$

where R is the bending angle Φ and A, B, C, D, E, F, G, and H are coded, respectively, for the length l of a single cavity, the width w of a single cavity, the height h of a single cavity, the thickness t of the expansion wall of a single cavity, the thickness t_1 of the nonretractable layer, the thickness t_2 of the thin leaf spring, the distance between the cavities I, and the total number of cavities N corresponding to the basic execution unit.

In the analysis of variance of the regression model and the significance test of model coefficients, the significance of each variable's influence on response value can be tested by determining F value and P value. As for the experiment model, $F = 78.51$ and $P < 0.0001$, indicating the difference is very significant. In addition, $R_2 = 0.9788$, Adj $R_2 = 0.9663$, Pre $R_2 = 0.9439$, and the variance difference is very small and close to 1, which indicates that the fitting degree of the model is fairly satisfactory. Therefore, this model can be used to analyze and predict the optimal extraction process of the bending angle Φ.

Then, based on response surface optimization test, analyze the effect of the interaction of AC, AD, AE, AF, AG, AH, BC, BD, BE, BF, BG, CD, CE, CH, DE, DF, DG, DH, EG, FG, FH, and GH on the bending angle Φ. The interaction of AB, BH, CF, and GH has a significant impact ($P < 0.05$), while the

interaction of *CG*, *EF*, and *EH* has no significant effect on bending angle Φ ($P > 0.05$). Therefore, the optimal extraction process can be obtained by analyzing the interaction of various factors, as shown in Table 3.

4. Analysis of the Mechanical Model

4.1. Mechanical Model Analysis of Silica Gel Material. Silica gel is a kind of nonlinear material with hyperelasticity, large deformation, and almost no change in volume (i.e., incompressible). Its common constitutive models include the Mooney–Rivlin model, Ogden model, and Yeoh model [39–42]. Among them, the Ogden model has high modeling accuracy and simple form; it can be verified by uniaxial tension, biaxial tension, and pure shear tests and can effectively solve the problem of large deformation of silica gel materials [43, 44]. Therefore, in this paper, the third-order Ogden constitutive model is used to analyze the nonlinear mechanics of the pneumatic soft-bodied bionic basic execution unit.

4.2. Establishment of the Mechanical Model for Pneumatic Soft-Bodied Bionic Basic Execution Unit. Based on the stress-strain relationship, the constitutive relation of silica gel material is established, and assuming that the silica gel material is isotropic and incompressible, the expressions of strain energy function, that is, (2) and (3) are as follows:

$$W = W(I_1, I_2, I_3), \tag{2}$$

$$\begin{cases} I_1 = \lambda_1^2 + \lambda_2^2 + \lambda_3^2, \\ I_2 = \lambda_1^2\lambda_2^2 + \lambda_2^2\lambda_3^2 + \lambda_1^2\lambda_3^2, \\ I_3 = \lambda_1^2\lambda_2^2\lambda_3^2, \end{cases} \tag{3}$$

where I_1, I_2, and I_3 are invariant of the deformation tensor and λ_1, λ_2, and λ_3 are the main elongation ratio in three directions of space.

According to the incompressibility of materials, (4) is rewritten as follows:

$$I_3 = \lambda_1^2\lambda_2^2\lambda_3^2 = 1. \tag{4}$$

Assuming that the material has no deformation in the direction of width $\lambda_3 = 1$, (5) and (6) can be obtained:

$$\lambda_1 = \frac{1}{\lambda_2}, \tag{5}$$

$$I_1 = I_2 = \lambda_1^2 + \frac{1}{\lambda_1^2} + 1. \tag{6}$$

Because silica gel material has nonlinear characteristics and its deformation state is different from that of small deformation materials, the relationship between stress and strain can be expressed by strain energy function.

The strain energy function of Ogden model is expressed as follows:

$$W = \sum_{i=1}^{n} \frac{\mu_i}{\alpha_i}\left(\lambda_1^{\alpha_i} + \lambda_2^{\alpha_i} + \lambda_3^{\alpha_i} - 3\right), \quad (0 \le n \le 3). \tag{7}$$

Table 3: Response test results of pneumatic soft-bodied bionic basic execution unit.

No.	Size	Value
1	Single cavity length l	27.41 mm
2	Single cavity width w	9.63 mm
3	Single cavity height h	14.92 mm
4	Thickness of expansion wall of single cavity t	0.83 mm
5	Nonretractable layer t_1	1.84 mm
6	Thickness of thin leaf spring t_2	0.34 mm
7	Cavity spacing i	1.34 mm
8	Total numbers of cavity N	11.23

By choosing the form of third-order parameters, $N = 3$, we can get

$$W = \frac{\mu_1}{\alpha_1}\left(\lambda_1^{\alpha_1} + \lambda_2^{\alpha_1} + \lambda_3^{\alpha_1} - 3\right) + \frac{\mu_2}{\alpha_2}\left(\lambda_1^{\alpha_2} + \lambda_2^{\alpha_2} + \lambda_3^{\alpha_2} - 3\right) + \frac{\mu_3}{\alpha_3}\left(\lambda_1^{\alpha_3} + \lambda_2^{\alpha_3} + \lambda_3^{\alpha_3} - 3\right), \tag{8}$$

where μ_i and α_i are the material parameters, $\mu_1 = -1.48$; $\alpha_1 = 1.43$; $\mu_2 = 1.94$; $\alpha_2 = 5.73$; $\mu_3 = 1.38$; $\alpha_3 = 1.54$.

The stress expression of silica gel material can be deduced as in

$$\sigma_i = \lambda_i\frac{\partial W}{\partial \lambda_i} - G = \sum_{j=1}^{N} \mu_j\lambda_i^{\alpha_j} - G, \quad (N = 3), \tag{9}$$

where G is hydrostatic pressure. $G = \mu_1\lambda_2^{\alpha_1} + \mu_2\lambda_2^{\alpha_2} + \mu_3\lambda_3^{\alpha_3} = \mu_1\lambda_3^{\alpha_1} + \mu_2\lambda_3^{\alpha_2} + \mu_3\lambda_3^{\alpha_3}$.

Therefore, (10)–(12) are established:

$$\sigma_1 = \sum_{j=1}^{N} \mu_j\lambda_i^{\alpha_j} - G = \mu_1\lambda_1^{\alpha_1} + \mu_2\lambda_1^{\alpha_2} + \mu_3\lambda_1^{\alpha_3} - G, \tag{10}$$

$$\sigma_2 = \sum_{j=1}^{N} \mu_j\lambda_i^{\alpha_j} - G = \mu_1\lambda_2^{\alpha_1} + \mu_2\lambda_2^{\alpha_2} + \mu_3\lambda_2^{\alpha_3} - G, \tag{11}$$

$$\sigma_3 = \sum_{j=1}^{N} \mu_j\lambda_i^{\alpha_j} - G = \mu_1\lambda_3^{\alpha_1} + \mu_2\lambda_3^{\alpha_2} + \mu_3\lambda_3^{\alpha_3} - G, \tag{12}$$

$\sigma_2 = \sigma_3 = 0$, as a result, $\lambda_2 = \lambda_3 = (1/\sqrt{\lambda_1})$.

Therefore, the following equationfd13 is established:

$$\sigma = \sigma_1 = \mu_1\left(\lambda_1^{\alpha_1} - \lambda_1^{-(\alpha_1/2)}\right) + \mu_2\left(\lambda_1^{\alpha_2} - \lambda_1^{-(\alpha_2/2)}\right) + \mu_3\left(\lambda_1^{\alpha_3} - \lambda_1^{-(\alpha_3/2)}\right). \tag{13}$$

Among them, the main elongation ratio of the basic execution unitfd14 is obtained:

$$\lambda_1 = \frac{\Phi}{\sin\Phi}, \tag{14}$$

where Φ represents the bending angle of the cavity structure of the basic execution unit under a certain pressure.

The bending angle Φ can be expressed as

$$\Phi = \frac{(w+i)N}{r}. \tag{15}$$

The expression of elastic modulus of thin leaf spring is as follows:

$$E = \frac{4L^3C}{bh^3}, \tag{16}$$

where C is the elastic constant of the thin leaf spring, L is the length of the thin leaf spring, b is the width of the thin leaf spring, and h is the thickness of the thin leaf spring.

The stress expression of thin leaf spring can be deduced as follows:

$$\xi = E\lambda_1. \tag{17}$$

At the end of the filling process, the wall pressure of the cavity structure of the basic executing unit can be considered as approximately equal. Assuming that the gas pressure in the cavity reaches P_i, the force analysis of the case shows that the moment balance formula of the pneumatic soft-bodied bionic basic execution unit, i.e. equation (18) is as follows:

$$P_i l^2 + P_i (w+t+i)^2 + P_i (h+t_1)^2 = \sigma t_1^2 + \xi t_2^2, \tag{18}$$

where σ is the internal stress of nonretractable layer and ξ is the internal stress of the thin leaf spring.

Finally, according to (14) to (18), the relationship between the bending angle Φ of the basic execution unit and the internal pressure in the case of maximum deformation is obtained as follows:

$$\Phi = \Phi(P_i). \tag{19}$$

5. Preparation of Pneumatic Soft-Bodied Bionic Basic Execution Unit

The 601 room temperature vulcanized silica gel, which is soft, strong, elastic, and difficult to tear and deform, is selected as the pneumatic soft-bodied bionic basic execution unit. For the determination of its hardness value, according to the actual work requirements of the pneumatic soft-bodied bionic basic execution unit, the body structure needs to have a certain strength and flexibility. If the hardness is lower (lower than Shore A15), the body structure is too soft, and if the hardness is higher (higher than Shore A25), the brittleness is relatively high, and fracture is easy to occur. Shore A15 to Shore A25 are generally more suitable for the research of soft robots. Through numerical simulation, a large inflation pressure (180 kpa) is applied to the finite element model with material properties in this hardness range. The calculation results are shown in Table 4.

The results show that the bending angle of the pneumatic soft-bodied bionic basic execution unit is too large from Shore A15 to Shore A17, and the expansion wall shows excessive deformation, when the material hardness value ranges from Shore A18 to Shore A25, the bending angle of the pneumatic soft-bodied bionic basic execution unit does not show excessive deformation, and the bending angle gradually decreases with the increase of hardness value. Therefore, Shore A18 is selected, which can meet the actual bending requirements and has the largest bending angle.

The specific preparation materials are shown in Table 5.

The preparation of basic execution unit needs to combine 3D printing technology, shape deposition, and soft lithography [21, 45, 46], including three casting operations, embedded thin leaf spring structure, and bonding operations.

(1) Design of mould structure: because of the combination of integrated mould and investment casting method, not only the preparation process is complex, but also the cost of the mould is high. Therefore, a set of combined moulds is designed to cast and prepare the basic execution unit, and the mould is shown in Figure 3.

(2) Embedding of the thin leaf spring structure: to ensure that the thin leaf spring structure stays as flat as possible in the middle of the nonretractable layer, it is necessary to divide the nonretractable layer into two parts; that is, when the 1/2 thickness of the nonretractable layer is completed and when it is about to solidify, the thin leaf spring structure should be laid flat on it. After further curing, the remaining 1/2 thickness of the nonretractable layer goes on being cast and built.

(3) Bonding method: the uncured liquid silica gel was used to bond the silica gel structure. It is verified that this method can not only ensure the attribute stability of the basic execution unit ontology structure but also integrate the combination structure into a whole, which has certain stability and reliability.

Finally, the physical model of pneumatic soft-bodied bionic basic execution unit is obtained as shown in Figure 4.

6. Experimental Test and Analysis

In order to lay the foundation for the further application of pneumatic soft-bodied bionic basic execution unit, it is necessary to comprehensively and deeply study its motion and dynamic characteristics. In this paper, the experimental test and analysis are carried out for the unidirectional and bidirectional forms of the pneumatic soft-bodied bionic basic execution unit. Among them, the pressure range inside of the cavity is 40 kpa to 180 kpa.

The main devices of the experiment include pneumatic soft-bodied bionic basic execution unit (unidirectional and bidirectional), pneumatic pump, electromagnetic reversing valve, pressure regulating valve, bending sensor, Arduino plate, and computer and force measuring test platform [47–50]; see Figure 5.

Table 4: Comparison of calculation results of the 601 room temperature vulcanized silica gel with different ranges of hardness value.

Hardness value (shore A)	Tensile strength (kpa)	Elongation (%)	Bending angle	Deformation analysis
15 to 17	890 to 1140	580 to 540	224° to 176°	Excessive
18 to 25	1250 to 1780	520 to 440	151° to 98°	Reasonable

Table 5: Preparation material.

Consumables for preparation	Details of materials
Cavity structure	601 room temperature vulcanized silica gel
Non-retractable layer structure	601 room temperature vulcanized silica gel
Thin leaf spring structure	Quenched 65Mn
Mould	PLA

(a) (b) (c) (d)

Figure 3: Mould structure. (a) Cavity mould main body. (b) Cavity mould upper cover. (c) Nonretractable layer mould. (d) Gas inlet forming plug.

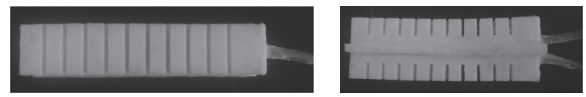

(a) (b)

Figure 4: Physical model of pneumatic soft-bodied bionic basic execution unit. (a) Unidirectional basic execution unit. (b) Bidirectional basic execution unit.

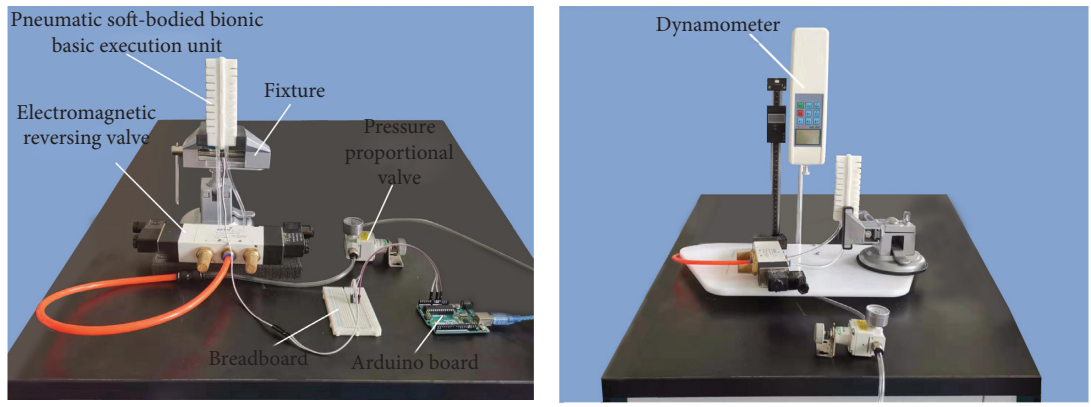

(a) (b)

Figure 5: Test platform of pneumatic soft-bodied bionic basic executing unit. Pneumatic soft-bodied bionic basic executing unit is demonstrated with bidirectional structure as an example. (a) Motion characteristics test. (b) Dynamic characteristic test.

6.1. *Motion Characteristics Analysis of Pneumatic Soft-Bodied Bionic Basic Execution Unit*

6.1.1. Motion Frequency Analysis. In the periodic motion process of the unidirectional pneumatic soft-bodied bionic basic execution unit, the cavity is inflated, and then the pressure is set to deflate immediately after end of inflation. Deflation ends when the basic execution unit reaches the flat state, so as to determine the time of cycle period and to complete the research of the unidirectional basic execution unit inflation and deflation; in the periodic motion process of the bidirectional pneumatic soft-bodied bionic basic

execution unit, it is necessary to select one cavity side to inflate. After the inflation is finished, the side cavity is deflated immediately, while the other side cavity is inflated. After the inflation is finished, the side cavity will deflate immediately until the end of deflation, and the bidirectional basic executing unit reaches the flat state. The state of inflation and deflation is shown in Figure 6.

After data acquisition, the sequence diagram of the inflation and deflation cycle of the pneumatic soft-bodied bionic basic execution unit is obtained as shown in Figure 7.

According to Figure 7, the change of motion cycle sequence of unidirectional and bidirectional pneumatic soft-bodied bionic basic execution units can be determined. Because the unidirectional basic execution unit only involves unidirectional motion, its motion time is shorter than that of the bidirectional basic execution unit. Among them, the cycle time of unidirectional basic execution unit is longer than that of the bidirectional basic execution unit, because the motion amplitude of unidirectional basic execution unit is larger than that of bidirectional basic execution unit under the same inflatable pressure. Besides, when the motion range of the basic execution unit increases with the increase of inflation pressure, the resilience force generated by the thin leaf spring structure also increases, which makes the motion recovery time of the basic execution unit gradually approach the motion bending time.

Then, according to the periodic motion of the pneumatic soft-bodied bionic basic execution units, the $P - f$ characteristic curves of the inflatable pressure and the bending angle of the basic execution units can be obtained, as shown in Figure 8.

According to Figure 8, it can be seen that the motion frequency of the pneumatic soft-bodied basic bionic execution unit increases first and then decreases gradually with the increase of the inflation pressure, which is caused by the gradual increase of its motion amplitude. When the motion amplitude is small, the inflation pressure increases and the motion frequency increases. When the motion amplitude is large, the motion frequency decreases gradually with the increase of the inflation pressure. Among them, the motion frequency of the unidirectional basic execution unit is higher than that of the bidirectional basic execution unit.

According to the $P - f$ characteristic curves of the basic execution unit, the empirical formula reflecting the change of the characteristic curves can be obtained. The expression of the empirical formula is as follows:

$$f(x) = p_1 \cdot x^4 + p_2 \cdot x^3 + p_3 \cdot x^2 + p_4 \cdot x + p_5. \quad (20)$$

Among them, the specific coefficients in the formula are shown in Table 6.

6.1.2. Bending Angle Analysis. Based on the bending sensor glued to the basic execution unit, the bending angle is collected by the program written in advance. The $P - \Phi$ characteristic curves of inflation pressure and bending angle can be obtained, as shown in Figure 9.

In Figure 9, it is shown that, under different inflation pressures, the bending angle of unidirectional and bidirectional basic execution units range from 0° to 148° and from 0° to 105°, respectively. Within this range, unidirectional and bidirectional basic execution units can guarantee the operation is in the best state, respectively. Among them, the characteristic curves change gradually from the initial linear to later the nonlinear, which is due to the expansion of the cavity structure to a certain extent, and the large reverse bending moment produced by the nonretractable layer silica gel body and the thin leaf spring structure. The bending angle of the bidirectional basic execution unit is smaller than that of the unidirectional basic execution unit because it also bears the reverse bending moment produced by the compressed side cavity body when bending. Therefore, the motion range of the unidirectional basic execution unit can meet the needs of most scenarios, while the bidirectional basic execution unit has some limitations, and the bidirectional basic execution unit should be selected according to the specific situation. In addition, when the inflatable pressure continues to increase, although the bending angle of the basic executive unit will continue to increase slowly, its motion characteristics will become worse, the executive ability will be weakened, and the operation effect will be affected to a certain extent.

In addition, the $P - \Phi$ characteristic curves of the pneumatic soft-bodied bionic basic execution unit can be expressed by empirical formula (20), and its specific proportional coefficients are shown in Table 7.

It is important to note that the unidirectional basic execution unit $P - \Phi$ characteristic curve is compared with the deformation model of the pneumatic soft-bodied bionic basic execution unit established by Odgen's third-order constitutive model, and the accuracy analysis result of the error bar is obtained, as shown in Figure 10.

According to Figure 10, it can be seen that the error bar analysis results confirm that the actual experimental and theoretical models exhibit small errors and high coincidence, which can verify the accuracy and reliability of the deformation model derived from the theory.

6.2. Analysis of Dynamic Characteristics. The dynamic test of the pneumatic soft-bodied bionic basic execution unit is carried out, as shown in Figure 11.

6.2.1. Dynamic Characteristic Analysis of Variable Bending Angle. The $P - M$ characteristic curves of inflation pressure and driving moment are obtained through representative data acquisition, as shown in Figure 12.

Figure 12 shows that the changing rule of the $P - M$ characteristic curves of unidirectional and bidirectional basic execution units are similar. The main difference is that the driving moment of bidirectional basic execution unit is relatively low, which is caused by the reaction moment produced by the compressed side cavity in the bidirectional basic execution unit. Besides, within a certain range of pressure change, the characteristic curves are approximately linear, and nonlinearity appears mainly in the case of low inflation pressure and high inflation pressure. Among them,

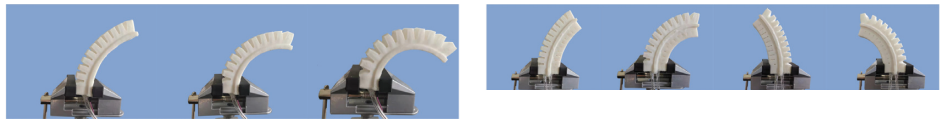

(a) (b)

Figure 6: Motion process of pneumatic soft-bodied bionic basic execution unit. (a) Unidirectional basic execution unit. (b) Bidirectional basic execution unit.

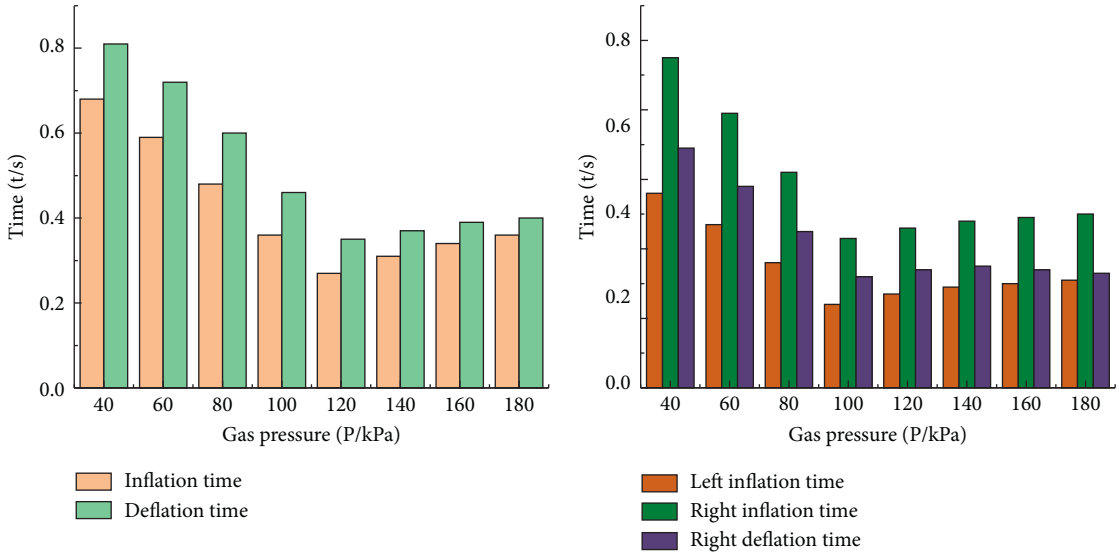

(a) (b)

Figure 7: Motion cycle sequence diagram of pneumatic soft-bodied bionic basic execution unit. (a) Unidirectional basic execution unit. (b) Bidirectional basic execution unit.

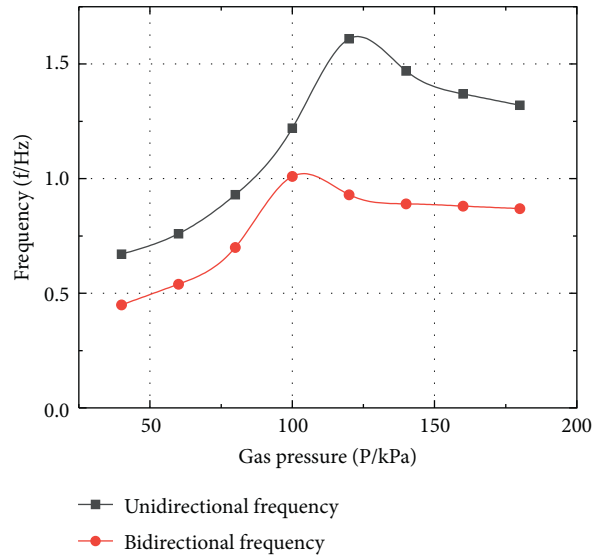

Figure 8: The $P - f$ characteristic curves of pneumatic soft-bodied bionic basic execution units.

when the inflation pressure is low, the main reason is that the thin leaf spring structure in the basic execution unit will produce some reaction moment, which offsets part of the driving moment; when the inflation pressure is high, the basic execution unit will produce extreme deformation, which leads to the change of its stress form.

The $P - M$ characteristic curves of the pneumatic soft-bodied bionic basic execution unit can be expressed by

Table 6: Empirical formula coefficients of $P-f$ characteristic curves.

Empirical formula coefficients	Unidirectional	Bidirectional
p_1	$2.669E-8$	$2.054E-8$
p_2	$-1.283E-5$	$-8.989E-6$
p_3	$2.082E-3$	$1.314E-3$
p_4	-0.1245	-0.06916
p_5	3.094	1.634

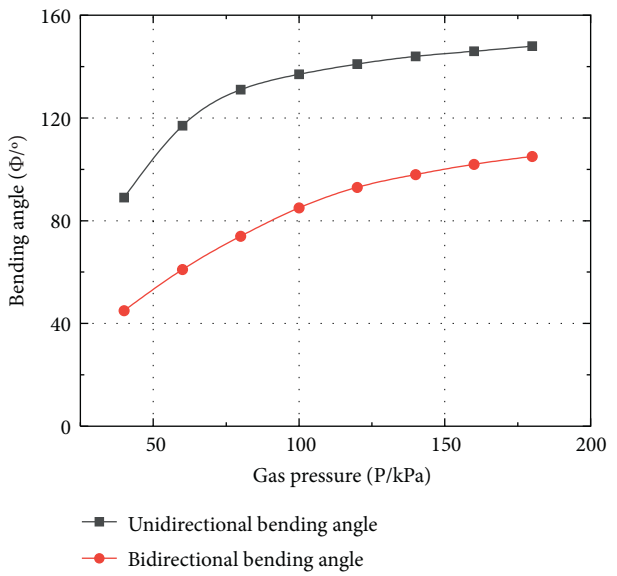

Figure 9: $P-\Phi$ characteristic curves of pneumatic soft-bodied bionic basic execution units.

Table 7: Empirical formula coefficients of $P-\Phi$ characteristic curves.

Empirical formula coefficients	Unidirectional	Bidirectional
p_1	$-5.623E-9$	$-8.108E-9$
p_2	$3.14E-6$	$4.19E-6$
p_3	$-6.696E-4$	$-8.124E-4$
p_4	0.06804	0.07552
p_5	-0.3905	-1.386

empirical formula (20), and its specific proportional coefficient is shown in Table 8.

6.2.2. Dynamic Characteristic Analysis of Fixed Bending Angle. The $P-M$ characteristic curves of inflation pressure and driving moment are obtained by representative data acquisition, as shown in Figure 13.

According to Figure 13, it can be seen that the distribution trends of the $P-M$ characteristic curves of the unidirectional and bidirectional pneumatic soft-bodied bionic basic units of fixed angle are almost the same, and their driving moment increases with the increase of the inflatable pressure. It should be noted that when the inflation pressure is low in the early stage, a large proportion of inflation is allocated to ensure that the basic execution unit reaches the set angle, which leads to the small increase of the driving moment in the early stage.

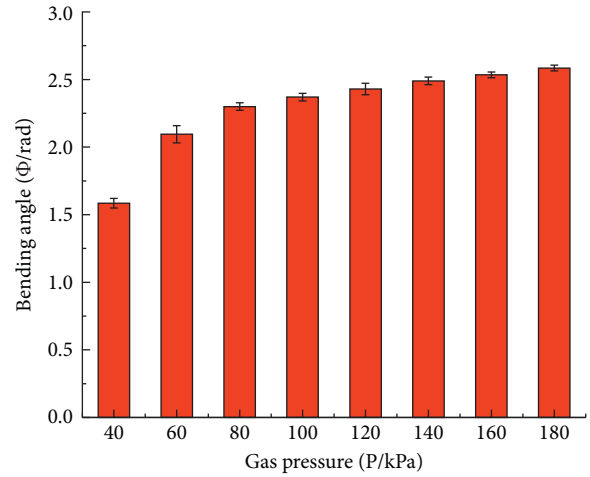

Figure 10: Error bar analysis of theoretical deformation model.

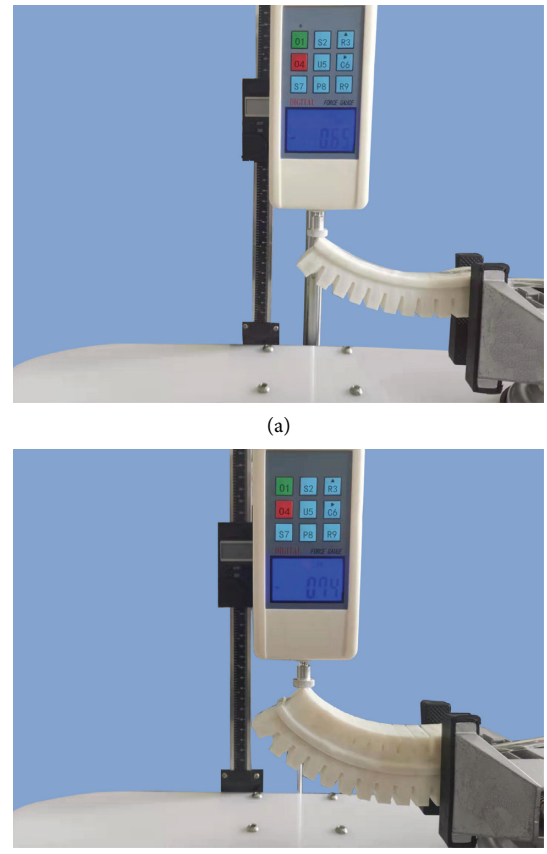

(a)

(b)

Figure 11: Torque measurement experiment of pneumatic soft-bodied bionic basic execution unit. (a) Unidirectional basic execution unit. (b) Bidirectional basic execution unit.

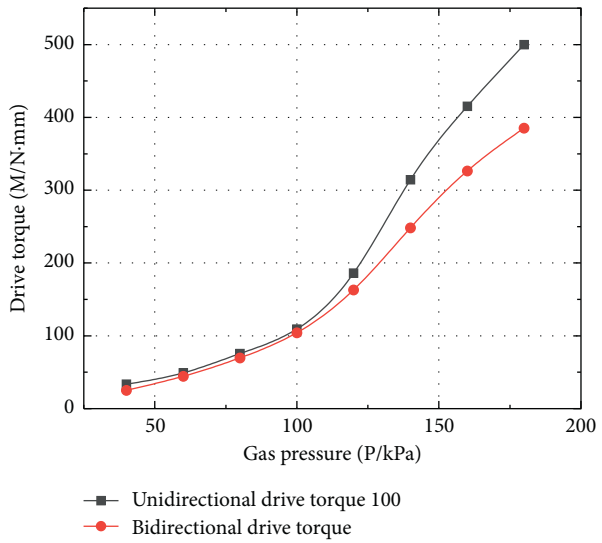

Figure 12: The $P-M$ characteristic curves of pneumatic soft-bodied bionic basic units for variable angle.

Table 8: Empirical formula coefficients of $P-M$ characteristic curves.

Empirical formula coefficients	Unidirectional	Bidirectional
p_1	$-4.833E-6$	$-2.919E-6$
p_2	$1.979E-3$	$1.184E-3$
p_3	−0.2543	−0.1497
p_4	13.89	8.562
p_5	−230.3	−146.5

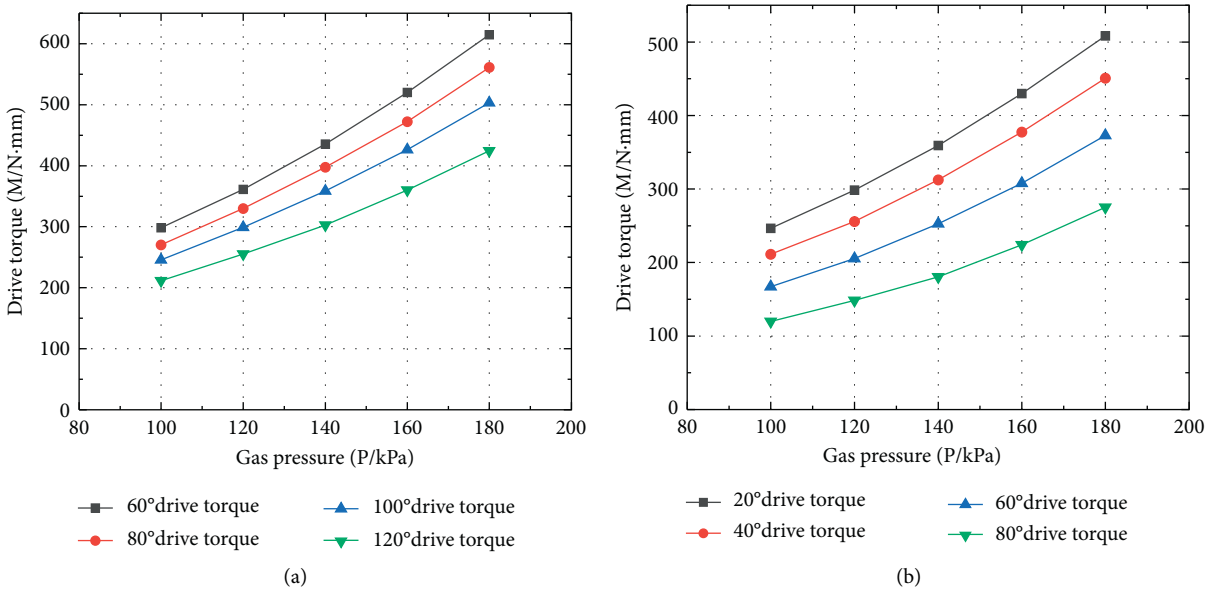

Figure 13: The $P-M$ characteristic curve of pneumatic soft-bodied bionic basic units for fixed angle. (a) Unidirectional basic execution unit. (b) Bidirectional basic execution unit.

7. Conclusions

(1) A pneumatic soft-bodied bionic basic execution unit with soft-rigid combination is designed for soft-bodied robots, soft-bodied manipulators, and other carriers that are suitable for underwater swimming, land crawling, and grasping.

(2) Using response surface analysis and numerical simulation algorithm, taking the maximum bending

angle, which is output of the pneumatic soft-bodied bionic basic execution unit, as the extraction target, the optimal combination of structural parameters is obtained.

(3) Based on Ogden's third-order constitutive model, a theoretical model for deformation analysis of pneumatic soft-bodied bionic basic execution unit is established, and the relationship between the bending angle of the basic execution unit and the inflation pressure is determined, which can provide a theoretical reference for the design and analysis of related soft-bodied robots.

(4) Through methods of 3D printing technology, shape deposition, and soft lithography, the soft-rigid combined physical models of unidirectional and bidirectional pneumatic soft-bodied bionic basic execution units were prepared. The key points are emphatically discussed, involving mould making, thin leaf spring structure embedding, and physical structure bonding.

(5) Based on the experimental platform of the motion and dynamic characteristics of the pneumatic soft-bodied bionic basic execution units, the characteristic curves of the motion frequency, bending angle, and driving moment of the basic execution unit and the corresponding empirical formulas are obtained by matching the motion and dynamic characteristics within a certain range according to the inflation pressure. The experimental data analysis shows that the deformation analysis model of the basic execution unit has high accuracy. It also proves that the physical model of the pneumatic soft-bodied bionic basic execution unit is feasible and can be used effectively as the pneumatic soft-bodied robot and the grasping actuator of the soft-bodied manipulator.

Data Availability

All data generated or analyzed during this study are included in this article.

Conflicts of Interest

The authors declare that there are no conflicts of interest regarding the publication of this paper.

Acknowledgments

This work was supported by the Institute of Robotics in Shenyang University of Technology and the National Natural Science Foundation of China (General Program) (Grant no. 51775354).

References

[1] A. D. Marchese, R. K. Katzschmann, and D. Rus, "A recipe for soft fluidic elastomer robots," *Soft Robotics*, vol. 2, no. 1, pp. 7–25, 2015.

[2] R. K. Katzschmann, A. D. Maille, D. L. Dorhout, and D. Rus, "Cyclic hydraulic actuation for soft robotic devices," in *Proceedings of the International Conference on Intelligent Robots and Systems (IROS)*, Daejeon, South Korea, October 2016.

[3] S. I. Rich, R. J. Wood, and C. Majidi, "Untethered soft robotics," *Nature Electronics*, vol. 12, no. 24, pp. 102–112, 2018.

[4] Y. F. Hao, Z. Y. Gong, Z. X. Xie et al., "Universal soft pneumatic robotic gripper with variable effective length," in *Proceedings of the 2016 35th Chinese Control Conference (CCC)*, Chengdu, China, July 2016.

[5] K. C. Galloway, K. P. Becker, B. Phillips et al., "Soft robotic grippers for biological sampling on deep reefs," *Soft Robotics*, vol. 3, no. 1, pp. 23–33, 2016.

[6] M. Kirby, R. L. Truby, D. J. Fitzgerald et al., "An integrated design and fabrication strategy for entirely soft, autonomous robots," *Nature*, vol. 536, no. 7617, pp. 451–455, 2016.

[7] W. Mosadegh, J. Y. Lee, H. Rodrigue et al., "Locomotion of inchworm-inspired robot made of smart soft composite (SSC)," *Bioinspiration & Biomimetics*, vol. 9, no. 4, Article ID 046006, 2014.

[8] K. Suzumori, S. Endo, T. Kanda et al., "A bending pneumatic rubber actuator realizing soft-bodied manta swimming robot," in *Proceedings of the IEEE International Conference on Robotics & Automation*, Rome, Italy, April 2007.

[9] A. D. Marchese, C. D. Onal, and D. Rus, "Autonomous soft robotic fish capable of escape maneuvers using fluidic elastomer actuators," *Soft Robotics*, vol. 1, no. 1, pp. 75–87, 2014.

[10] M. T. Tolley, R. F. Shepherd, B. Mosadegh et al., "Untethered soft robot," *Soft Robotics*, vol. 1, no. 2, pp. 41–51, 2014.

[11] A. D. Marchese, R. K. Katzschmann, and D. L. Rus, "Whole arm planning for a soft and highly compliant 2D robotic manipulator," in *Proceedings of the International Conference On Intelligent Robots & Systems*, Chicago, IL, USA, September 2014.

[12] S. Li, D. M. Vogt, D. Rus et al., "Fluid-driven origami-inspired artificial muscles," *Proceedings of the National Academy of Sciences*, vol. 114, Article ID 201713450, 2017.

[13] S. Liming, L. Tingyu, and X. I. Zuoyan, "Analysis and experiment of actuating method for pneumatic soft crawling robot," *Chinaese Hydraulic & Pneumatics*, vol. 11, pp. 99–103, 2018.

[14] B. T. Phillips, K. P. Becker, S. Kurumaya et al., "A dexterous, glove-based teleoperable low-power soft robotic arm for delicate deep-sea biological exploration," *Scientific Reports*, vol. 8, no. 18, pp. 38–46, 2018.

[15] J. Frame, N. Lopez, O. Curet, and E. D. Engeberg, "Thrust force characterization of free-swimming soft robotic jellyfish," *Bioinspiration & Biomimetics*, vol. 13, Article ID 064001, 2016.

[16] Y. Jiantao, C. Xinbo, C. Juntao et al., "Design and motion analysis of a wheel-walking bionic soft robot," *Journal of Mechanical Engineering*, vol. 55, no. 5, pp. 27–35, 2019.

[17] M. J. Bishop and S. Kota, "Towards snake-like soft robots: design of fluidic fiber-reinforced elastomeric helical manipulators," in *Proceedings of the International Conference on Intelligent Robots and Systems (IROS)*, Tokyo, Japan, November 2013.

[18] J. B. Moser, G. Krishnan, C. Kim, and S. Kota, "Design of soft robotic actuators using fluid-filled fiber-reinforced elastomeric enclosures in parallel combinations," in *Proceedings of the International Conference Intelligent Robots And Systems*, IEEE/RSJ, Algarve, Portugal, October 2012.

[19] B. Mosadegh, P. Polygerinos, C. Keplinger et al., "Soft robotics: pneumatic networks for soft robotics that actuate rapidly," *Advanced Functional Materials*, vol. 24, no. 15, 2014.

[20] M. Luo, W. Tao, F. Chen et al., "Design improvements and dynamic characterization on fluidic elastomer actuators for a soft robotic snake," in *Proceedings of the International Conference Intelligent Robots And Systems*, IEEE/RSJ, Chicago, IL, USA, September 2014.

[21] B. N. Peele, T. J. Wallin, H. Zhao, and R. F. Shepherd, "3D printing antagonistic systems of artificial muscle using projection stereolithography," *Bioinspiration & Biomimetics*, vol. 10, no. 5, Article ID 055003, 2015.

[22] F. Connolly, P. Polygerinos, C. J. Walsh, and K. Bertoldi, "Mechanical programming of soft actuators by varying fiber angle," *Soft Robotics*, vol. 2, no. 1, pp. 26–32, 2015.

[23] C. Pengzhan, Z. Wuwei, and J. Zet, "Design and control of soft pneumatic fiber-reinforcement actuator," *Journal of Nanjing University of Science and Technology*, vol. 2, no. 20, pp. 218–222, 2016.

[24] A. Jusufi, M. V. Daniel, R. J. Wood, and G. V. Lauder, "Undulatory swimming performance and body stiffness modulation in a soft robotic fish-inspired physical model," *Soft Robotics*, vol. 4, no. 11, pp. 11–19, 2017.

[25] S. Li-ming, X. Zuoyan, and L. Tingyu, "Design and fabrication of multi-chamber biomimetic pneumatic soft actuators," *Chinese Journal of Engineering Design*, vol. 5, pp. 31–37, 2017.

[26] F. Jizhuang, Y. Qingguo, Y. Bowen, and Z. Jie, "Development of a joint-like pneumatic actuator applied to soft frog-inspired swimming robot," *Robot*, vol. 40, no. 5, pp. 4–12, 2018.

[27] L. Chen, C. Yang, H. Wang, J. S. Dai, and R. Kang, "Design and modeling of a soft robotic surface with hyperelastic material," *Mechanism and Machine Theory*, vol. 130, pp. 109–122, 2018.

[28] O. Azami, D. Morisaki, T. Miyazaki et al., "Development of the extension type pneumatic soft actuator with built-in displacement sensor," *Sensors and Actuators A: Physical*, vol. 300, Article ID 111623, 2019.

[29] M. A. Saleh, M. A. Soliman, M. A. Mousa et al., "Design and implementation of variable inclined air pillow soft pneumatic actuator suitable for bioimpedance applications," *Sensors and Actuators A: Physical*, vol. 314, Article ID 112272, 2020.

[30] I. Kaymaz and C. A. Mcmahon, "A response surface method based on weighted regression for structural reliability analysis," *Probabilistic Engineering Mechanics*, vol. 20, no. 1, pp. 11–17, 2005.

[31] H. Majdi, J. A. Esfahani, and M. Mohebbi, "Optimization of convective drying by response surface methodology," *Computers and Electronics in Agriculture*, vol. 156, pp. 574–584, 2019.

[32] G. Salih and Y. Aytac, "Optimization of cutting parmeters using the response surface method," *Sigma Journal of Engineering and Natural Sciences*, vol. 36, no. 1, pp. 113–121, 2018.

[33] S. Sundari and S. Sukumar, "Prediction model for optimized self-compacting concrete with fly ash using response surface method based on fuzzy classification," *Neural Computing and Applications*, vol. 23, no. 6, pp. 113–121, 2018.

[34] A. I. Khuri and S. Mukhopadhyay, "Response surface methodology," *WIREs Computational Statistics*, vol. 2, 2010.

[35] Y. T. Kao, Y. Zhang, and J. Wang, "Bending behaviors of 3D-printed bi-material structure: experimental study and finite element analysis," *Additive Manufacturing*, vol. 16, 2017.

[36] W.-M. Chen, T. Lee, P. V.-S. Lee, J. W. Lee, and S.-J. Lee, "Effects of internal stress concentrations in plantar soft-tissue-a preliminary three-dimensional finite element analysis," *Medical Engineering & Physics*, vol. 32, no. 4, pp. 324–331, 2010.

[37] S. Kindo, R. Vashistha, S. Raj et al., "Selection and validation of hyperelastic finite element model for analysis of silicone rubber," *AIP Conference Proceedings*, vol. 12, no. 1978, Article ID 470006, 2018.

[38] T. Jiang, J. Shang, L. Tang, and Z. Wang, "Thickness optimization of auricular silicone scaffold based on finite element analysis," *Journal of the Mechanical Behavior of Biomedical Materials*, vol. 53, pp. 397–402, 2016.

[39] Y. Mei, B. Stover, N. A. Kazerooni et al., "A comparative study of two constitutive models within an inverse approach to determine the spatial stiffness distribution in soft materials," *International Journal of Mechanical Sciences*, vol. 140, 2018.

[40] S. K. Panda and M. L. Buist, "A finite nonlinear hyper-viscoelastic model for soft biological tissues," *Journal of Biomechanics*, vol. 69, 2018.

[41] K. Matous, M. G. D. Geers, and V. G. Kouznetsova, "A review of predictive nonlinear theories for multiscale modeling of heterogeneous materials," *Journal of Computational Physics*, vol. 330, no. 126, pp. 192–220, 2017.

[42] Y. Staudt, C. Odenbreit, and J. Schneider, "Failure behaviour of silicone adhesive in bonded connections with simple geometry," *International Journal of Adhesion and Adhesives*, vol. 82, 2018.

[43] M. S. Rogachev, Y. I. Shtern, and M. Yu, "Modeling of thermal expansion of the multisectional generator thermoelements," in *Proceedings of the Conference of Russian Young Researchers in Electrical and Electronic Engineering*, IEEE, Moscow, Russia, February 2018.

[44] S. M. R. Khalili, M. Botshelcanan Dehlcordi, E. Carrera, and M. Shariyat, "Non-linear dynamic analysis of a sandwich beam with pseudoelastic SMA hybrid composite faces based on higher order finite element theory," *Composite Structures*, vol. 96, pp. 243–255, 2013.

[45] O. D. Yirmibesoglul, J. Morrow, S. Walker et al., "Direct 3D printing of silicone elastomer soft robots and their performance comparison with molded counterparts," *Soft Robotics*, vol. 4, no. 24, pp. 295–302, 2018.

[46] M. Launhardt, N. Ebel, M. Kondruweit et al., "Developing a patient individualized flexible silicone implant using SLS and vacuum mould casting," *AIP Conference Proceedings*, vol. 15, pp. 115–124, 2019.

[47] Q. Xu, J. Liu, and L. Qu, "Dynamic modeling for silicone beams using higher-order ANCF beam elements and experiment investigation," *Multibody System Dynamics*, vol. 46, no. 224, pp. 122–137, 2019.

[48] G. Agarwal, N. Besuchet, and B. Audergon, "Stretchable materials for robust soft actuators towards assistive wearable devices," *Scientific Reports*, vol. 6, pp. 324–342, 2016.

[49] C. Arnab and C. Christian, "Tissue anisotropy modeling using soft composite materials," *Applied Bionics and Biomechanics*, vol. 2018, Article ID 4838157, 9 pages, 2018.

[50] B. Ma, Z. Liu, F. Jiang, Y. Yan, J. Yuan, and S. Bu, "Vehicle detection in aerial images using rotation-invariant cascaded forest," *IEEE Access*, vol. 7, pp. 59613–59623, 2019.